Comparisons between LES and wind tunnel hot-wire measurements of a NACA 0015 airfoil

Zhu, Wei Jun; Shen, Wen Zhong; Bertagnolio, Franck; Sørensen, Jens Nørkær

Published in:
Proceedings of EWEA 2012 - European Wind Energy Conference & Exhibition

Publication date:
2012

Document Version
Publisher's PDF, also known as Version of record

Comparisons between LES and wind tunnel hot-wire measurements of a NACA 0015 airfoil

Wei Jun Zhu
Technical University of Denmark
wjzh@dtu.dk

Wen Zhong Shen
Technical University of Denmark
wzsh@dtu.dk

Franck Bertagnolio
Technical University of Denmark
frba@dtu.dk

Jens Nørkær Sørensen
Technical University of Denmark
jnso@dtu.dk

Abstract

Large-eddy simulations (LES) are carried out for flow over a NACA 0015 airfoil at AoA = 8^o and chord based Reynolds number of 1.71×10^6. To accurately simulate the complex flow at the suction side of the airfoil, a reasonably large number of grid points are required. The computational mesh is constructed in a wind tunnel similar as the condition where the experiments were carried out. The goal of this study is to validate the LES model against detailed measurements. The simulations are performed with in-house EllipSys3D code on high performance computers. Numerical study are focused on the stability and accuracy of the LES simulations on various mesh configurations. The spanwise grid spacing was found important to produce correct flow disturbance along the airfoil span, which further affects the turbulent energy distribution.

Keywords Large eddy simulation, turbulent flow

1 Introduction

Computational fluid dynamics (CFD) has entered into its mature stage. Different techniques exist to model turbulent flows: the Reynolds-averaged Navier-Stokes (RANS) method, the detached eddy simulation (DES), the large eddy simulation (LES) and the direct numerical simulation (DNS). The RANS techniques are most popular for solving engineering based flow problems. One has the alternative to choose one equation models that are the Baldwin-Barth model [1] and the Spalart-Allmaras model [2], and the two equation models that are the k-epsilon model [3] and the k-omega model [4]. A more advanced method that combines RANS and LES is the DES method [5]. Comparing with RANS, DES is much more convincing to resolve highly separated turbulent flows. In LES, large eddies are solved explicitly and the smaller eddies are treated implicitly using the sub-grid-scale (SGS) models. LES does not resolve full range of turbulence scales, but it solves scales much wider range than RANS. The use of LES is a compromise between limited computer resource and numerical accuracy. As the grid becomes finer, the SGS Reynolds stress is smaller, the method is identical to DNS when the grid density is high enough to resolve the smallest eddy structures.

The increase of computer power and memory storage have raised the interest of LES applications. LES appears to be a potential numerical tool that can handle complex turbulent flow problems. The foundation works of Smagorinsky [6], Lilly [7] and Deardorff [8] were aimed at weather forecasts. For flow at smaller scales, such as turbulent airfoil flows, some modified LES models were proposed. The method for modeling the SGS stress tensor is seen in Bardina et al. [9]. Model of Ta Phuoc [10] and Sagaut [11] is an extension of the Smagorinsky model as well. The eddy viscosity is a function of vorticity, shear strain tensor and kinetic energy, therefore it is called mixed scale eddy viscosity model. Such approach is seen in Mary and Sagaut [12] who has simulated flow over an airfoil near stall. It was found that the simulated mean and fluctuating velocity profiles compare favourably with experimental data. It was suggested that the streamwise, the wall normal and the spanwise mesh resolution in terms of wall units must satisfy the grid size constrains: $\Delta x^+<50$, $\Delta y^+\approx2$, $\Delta z^+\approx20$, respectively. On the other hand, the values suggested by [13] are $50<\Delta x^+<150$, $\Delta y^+\approx1$, $15<\Delta z^+<40$. For comparison, the criteria used for DNS is: $10<\Delta x^+<20$, $\Delta y^+\approx1$, $5<\Delta z^+<10$. In the above criteria, the limitation of the spanwise spacing is even more critical than in the streamwise direction. In the present paper, the mixed eddy viscosity model is used to investigate turbulent flow over a NACA 0015 airfoil. Numerical simulations are conducted in a wind tunnel with similar geometry as the experimental setup. Effect of grid spacing in the spanwise direction are investigated.

2 Numerical method

2.1 Governing equations

In LES the filtered Navier-Stokes equations is defined as

$$\frac{\partial \overline{U}_i}{\partial t} + \frac{\partial \left(\overline{U}_i \overline{U}_j\right)}{\partial x_j} = -\frac{1}{\rho}\frac{\partial \overline{P}}{\partial x_i} + \nu \frac{\partial^2 \overline{U}_i}{\partial x_j^2} + \frac{\partial \tau_{ij}}{\partial x_j} \quad (1)$$

$$\frac{\partial \overline{U}_i}{\partial x_i} = 0 . \quad (2)$$

where the first filter is identified by a bar ($\bar{}$). The solutions obtained from Equations (1) and (2) are filtered due to the finest grid level use in computation.

The flow velocity can be written as $U_i = \overline{U}_i + U_i'$, where $\overline{U}_i$ represents the large scale part and U_i' is its small scale part. The large scales of flow are simulated where the small scales are modelled by the sub-grid-scale (SGS) model. The term that requires modelling is the SGS stress

$$\tau_{ij} = \overline{U}_i\overline{U}_j - \overline{U_i U_j} = \left(\overline{U}_i\overline{U}_j - \overline{\overline{U}_i\overline{U}_j}\right) - \left(\overline{\overline{U}_i U_j' + U_i'\overline{U}_j}\right) - \overline{U_i'U_j'} , \quad (3)$$

The turbulent stresses are modelled with an eddy viscosity

$$\tau_{ij} = \nu_t\left(\frac{\partial \overline{U}_i}{\partial x_j} + \frac{\partial \overline{U}_j}{\partial x_i}\right) - \frac{2}{3}k\delta_{ij} . \quad (4)$$

The eddy viscosity is determined by the mixed scale turbulence model introduced by Ta Phuoc [10]

$$\nu_t = C\left|\overline{\vec{\omega}}\right|^{\alpha} k^{(1-\alpha)/2}\Delta^{(1+\alpha)} , \quad (5)$$

where $\Delta = \left(\Delta_x\Delta_y\Delta_z\right)^{1/3}$ is an average grid size, and α is a parameter that takes values in the range between 0 and 1. The turbulent kinetic energy can be estimated by using the test filter

$$k = \frac{1}{2}\sum_{j=1}^{3}\left(U_j - \overline{U}_j\right)^2 \approx \frac{1}{2}\sum_{j=1}^{3}\left(\overline{U}_j - \tilde{\overline{U}}_j\right)^2 , \quad (6)$$

where $\tilde{\overline{U}}_j$ is velocity resulted from the test filter. Assuming similarity between two grid levels, the test filter is based on the coarser mesh that is double as the finest mesh. The model Eq. (5) becomes a pure vorticity based model in the case when $\alpha = 1$,

$$\nu_t = C\left|\overline{\vec{\omega}}\right|\Delta^2 , \quad (7)$$

and it becomes the Bardina model [9] in the case when $\alpha = 0$,

$$\nu_t = Ck^{1/2}\Delta . \quad (8)$$

From studies on the model parameter, it was found that the model generally performs best when the parameter is chosen to be $\alpha = 0.5$,

$$\nu_t = C\left|\overline{\vec{\omega}}\right|^{1/2} k^{1/4}\Delta^{3/2} , \quad (9)$$

with $C = 0.04$. Therefore, this model is used in our computations for turbulent flows.

2.2 The flow solver

The EllipSys code [14,15,16] has been developed for solving general incompressible flows. The solver is based on a second-order finite volume method where the multi-grid strategy is used for solving the pressure correction equation. The code solves the velocity-pressure coupling equations with the SIMPLE/SIMPLEC/PISO method. The momentum equations are first solved with a known pressure as a prediction of the solution and the continuity equation is used as a constraint on the predicted velocity to obtain the pressure correction equation. In the predictor step, the momentum equations are solved by the second-order backward scheme in time and second-order central differences in space. The QUICK upwind scheme is used for the convective terms instead of using central schemes. In the corrector step, the improved Rhie-Chow interpolation [17] is applied to suppress numerical oscillations from velocity-pressure decoupling. Also, the improved SIMPLEC scheme for collocated grids [18] is used such that the solution is independent of the relaxation parameters and the time-step.

The differential form of NS equations are transformed into a curvilinear coordinate system aligned with the local grid lines. In 3D case, the metric expressions of the partial differentials are

$$\frac{\partial}{\partial x} = \frac{1}{J}\left(\frac{\partial}{\partial \xi}\alpha_{\xi x} + \frac{\partial}{\partial \eta}\alpha_{\eta x} + \frac{\partial}{\partial \zeta}\alpha_{\zeta x}\right)$$

$$\frac{\partial}{\partial y} = \frac{1}{J}\left(\frac{\partial}{\partial \xi}\alpha_{\xi y} + \frac{\partial}{\partial \eta}\alpha_{\eta y} + \frac{\partial}{\partial \zeta}\alpha_{\zeta y}\right) \quad (10)$$

$$\frac{\partial}{\partial z} = \frac{1}{J}\left(\frac{\partial}{\partial \xi}\alpha_{\xi z} + \frac{\partial}{\partial \eta}\alpha_{\eta z} + \frac{\partial}{\partial \zeta}\alpha_{\zeta z}\right)$$

where $\alpha_{()}$ are the partial differentials between the two coordinates and J is the Jacobian.

Inserting the above metric expressions into the U-momentum equation by a coordinate transformation $(x, y, z) \rightarrow (\xi, \eta, \zeta)$ yields

$$\frac{\partial \rho J U}{\partial t} + \frac{\partial C_1 U}{\partial \xi} + \frac{\partial C_2 U}{\partial \eta} - \frac{\partial}{\partial \xi}\left(\frac{\mu}{J}\beta_{11}U_\xi\right) - \frac{\partial}{\partial \eta}\left(\frac{\mu}{J}\beta_{22}U_\eta\right) - \frac{\partial}{\partial \xi}\left(\frac{\mu}{J}\left(\beta_{12}U_\eta + \omega_1\alpha_{\xi x} + \omega_2\alpha_{\xi y}\right)\right) - \frac{\partial}{\partial \eta}\left(\frac{\mu}{J}\left(\beta_{21}U_\xi + \omega_1\alpha_{\eta x} + \omega_2\alpha_{\eta y}\right)\right) + \frac{\partial P\alpha_{\xi x}}{\partial \xi} + \frac{\partial P\alpha_{\eta x}}{\partial \eta} = JS_U \quad (11)$$

where U is a velocity component, S_U is the volume source. The coefficients in Equation (11) are

$$\begin{aligned} C_1 &= \rho U\alpha_{\xi x} + \rho V\alpha_{\xi y} \\ C_2 &= \rho U\alpha_{\eta x} + \rho V\alpha_{\eta y} \\ \beta_{11} &= \alpha_{\xi x}\alpha_{\xi x} + \alpha_{\xi y}\alpha_{\xi y} \\ \beta_{12} &= \alpha_{\xi x}\alpha_{\eta x} + \alpha_{\xi y}\alpha_{\eta y} \\ \beta_{21} &= \alpha_{\eta x}\alpha_{\xi x} + \alpha_{\eta y}\alpha_{\xi y} \\ \beta_{22} &= \alpha_{\eta x}\alpha_{\eta x} + \alpha_{\eta y}\alpha_{\eta y} \\ \omega_1 &= \alpha_{\xi x}U_\xi + \alpha_{\eta x}U_\eta \\ \omega_2 &= \alpha_{\xi x}V_\xi + \alpha_{\eta x}V_\eta \end{aligned} \quad (12)$$

The other two momentum equations have similar expressions, the reader is referred to [16] for more details.

3 Numerical simulations

This section presents results from numerical simulations in the wind tunnel. Numerical results are compared with the wind tunnel measurements [19] carried out at LM wind tunnel.

3.1 Computational mesh

The LM Wind Power wind tunnel has the actual test section dimensions: 1.35 m in width, 2.70 m in height and 7 m in length. A NACA 0015 airfoil section of 0.9 m chord is placed across the width of the tunnel. For numerical simulations, we use similar configuration as the experiment. As drawn in Figure 1, the domain height is H = 2.70 m. The total length of the tunnel is 30 m that is considered for numerical stability at inlet and outer boundary. The airfoil chord is 0.9 m and it is placed in the centre of the computational domain. However, the spanwise extension is only 2% of the chord length. The reason of choosing a small span is due to the requirement of small grid spacing in the spanwise. Results obtained from a larger span-width will be shown later. The streamwise, the wall normal and the spanwise mesh resolution in terms of wall units shall be small enough to satisfy: $\Delta x^+ \leq 50$, $\Delta y^+ \approx 2$, $\Delta z^+ \leq 20$, as mentioned earlier. To meet this criteria, the present mesh has an off-wall cell size between 1×10^{-5} to 5×10^{-5} chord length. For a span of 2% airfoil chord, the maximum grid-spacing measured in wall unites, is $\Delta x^+ \approx 30$, $\Delta y^+ \approx 2$, and $\Delta z^+ \approx 20$ in the streamwise, wall normal and spanwise directions, respectively. Thus, the maximum Δx^+ is 15 times of Δy^+ and Δz^+ is 10 times of Δy^+. Periodic boundary condition is used at the end of the two spanwise directions, wall boundary condition is used for the top and bottom sides, inflow and outflow boundaries are set for inlet and outlet.

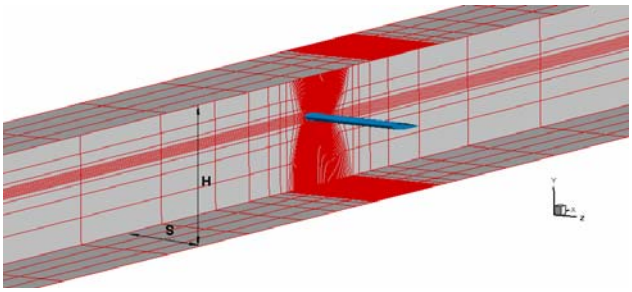

Figure 1. Numerical mesh configuration (plot at every 8th grid lines).

3.2 LES results and comparisons

The spanwise iso-surface vorticity is plotted in Figure 2 after the flow is fully established. It is observed that the flow separation occurs near the leading edge at its suction surface. At 8 degrees of angle of attack, the flow is near stall. The vorticity plot consists of eddies structures of varying size, indicating the complexity of turbulent boundary layer at suction side. At the trailing edge

position of x/c=0.91, the averaged horizontal and vertical velocity components along the wall normal direction are compared with measured data. Figure 3. has shown good agreement between vertical velocity comparison. The horizontal velocity has general agreement with the experiment data. The flow is fully separated at trailing edge position x/c=0.91, the discrepancy between comparison indicates that better grid resolution in streamwise direction might needed.

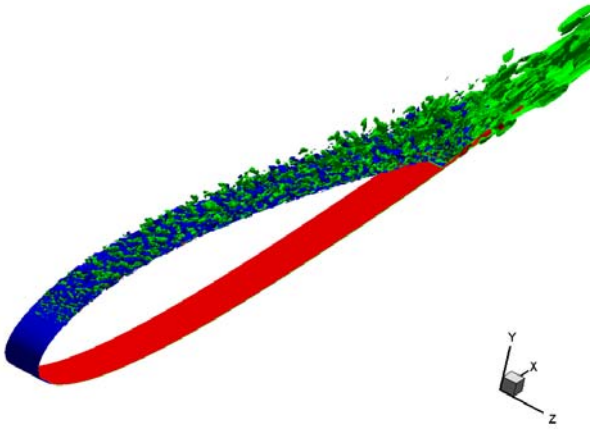

Figure 2. Instantaneous iso-surface plot of spanwise vorticity (ω_z) plot at a Reynolds number of 1.71×10^6 and an angle of attack of 8^o.

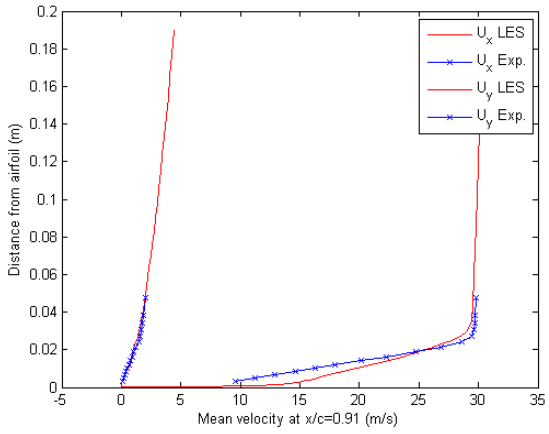

Figure 3. Mean velocities compared with experiments.

Time history data are recorded at each time iteration near the trailing edge along the wall normal direction. This allows us to compare the horizontal and vertical turbulent stresses against the hot-wire measurements. In Figure 4, the turbulent stresses are plotted together along the wall normal direction at the trailing edge position of x/c=0.91. The agreements between the simulations and the measurements are satisfied. Results are also shown for the spanwise velocity component. In Figure 5, the mean velocity has large fluctuation in the boundary layer and becomes zero at larger off-wall distance. This can be seen from the plot of turbulent stress where the $<u_z u_z>$ component is even larger than the vertical turbulent stress, as shown in Figure 4 and Figure 5. Even though the time-averaged velocity in the spanwise direction is zero, but the velocity fluctuation in the boundary layer is significant. Energy cascades from large to small eddies due to the spanwise disturbance, large eddies convected from the main stream were disturbed, where small eddies are generated which receive energy from larger eddies.

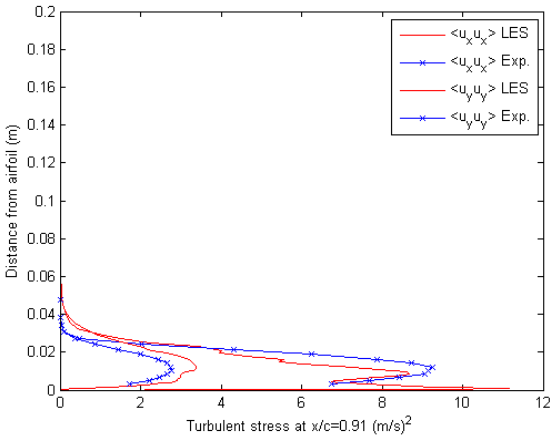

Figure 4. Turbulent stresses compared with experiments.

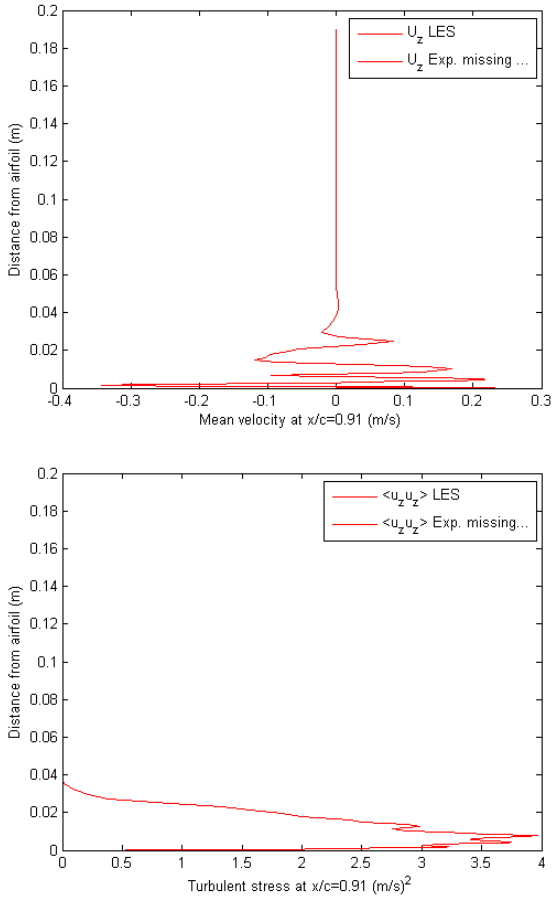

Figure 5. Spanwise mean velocity and turbulent stress.

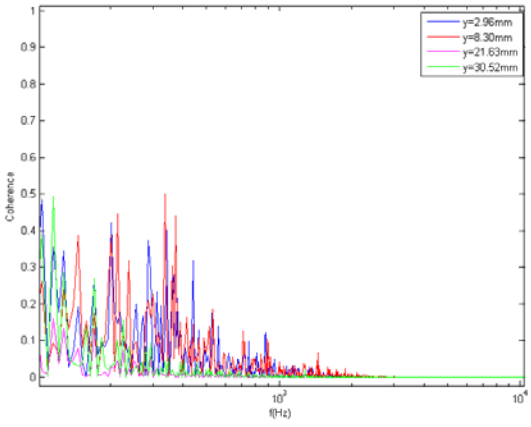

Figure 6. Coherence of pressure and streamwise velocity.

The coherence function of two signals of $S_1(f)$ and $S_2(f)$ is given by

$$Coh_{12}(f) = \frac{|S_{12}(f)|^2}{S_1(f)S_2(f)} \leq 1 \qquad (13)$$

where $S_1(f)$ and $S_2(f)$ are the spectral densities of two signals, $S_{12}(f)$ is the cross spectral density between two signals. Signals are linearly dependent if the coherence is 1, and it becomes zero when they are statistically independent, such that they are non-coherent. The coherence of pressure and streamwise velocity is calculated and results are shown in Figure 6. It can be seen that the two signals are coherent at the four tested boundary layer positions. At high frequencies, they are less coherent because of strong numerical dissipations and under-resolved small eddies. Similar tendency can be found from the phase difference of two signals by using equation (14).

$$\Delta\phi_{12}(f) = \arctan\left[\mathrm{Im}(S_{12}(f)/\mathrm{Re}(S_{12}(f))\right] \qquad (14)$$

The integral time scale can be calculated as

$$R_{ii}(\tau) = \lim_{T\to\infty}\frac{1}{2T}\int_{-T}^{T} u_i(t)u_i(t+\tau)dt \qquad (15)$$

For finite number of LES data, we have

$$R_{ii}(m) = \frac{1}{N}\sum_{n=1}^{N-m+1} u_i(n)u_i(n+m-1) \qquad (16)$$

The first cross-point at zero y-axis corresponds an integral time scale. As seen in Figure 7, the time scale increases as boundary layer thickness increase where the wave-length becomes longer.

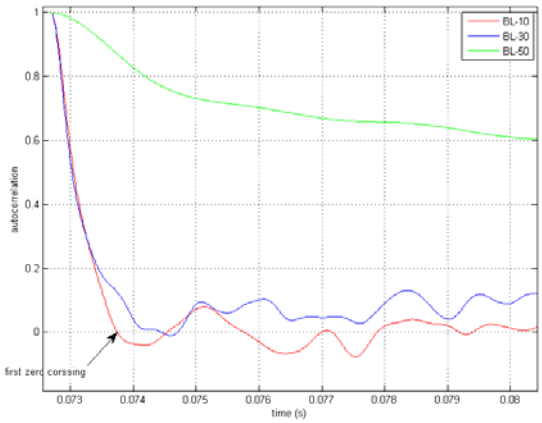

Figure 7. Autocorrelation at BL sample points. At positions of 10%, 30% and 50% of boundary layer thickness.

Multiplying the integral time scale by the mean velocity gives the integral length scale. The integral length scales are compared with experiment. In Figure 7, the solid lines are the length scales in mean flow direction, and the dot lines are the length scales in cross flow direction. The LES data have general agreement with the experimental data.

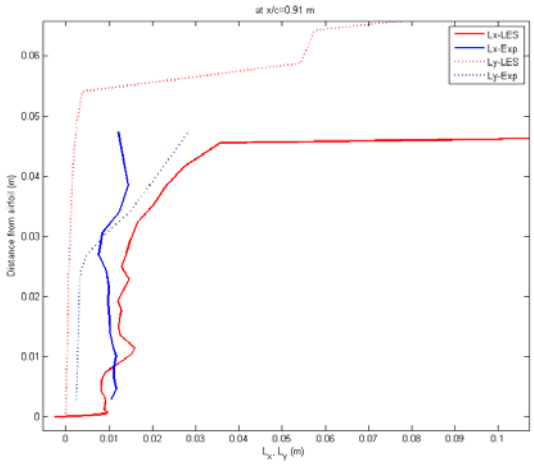

Figure 8. Turbulence integral length scales.

To investigate the effect from the spanwise grid resolution, LES was carried out using a computational mesh that is stretched 10 times in the spanwise direction. This means that the span is 20% of chord and $\Delta z+ \approx 200$. The resulted mean velocity still agrees well with experimental data. But the streamwise turbulent stress is far more larger than the measurement. Similar results was obtained from 2D simulation. In Figure 10, 2D simulation also resulted in good agreement with mean velocity, however, the turbulent stress in streamwise direction is more than 5 times larger than measured data. From the vorticity plots in Figure 11, the vortex size from 2D simulation is seen much larger than the 3D case. Due to the weak effect of spanwise disturbance, the large eddies are not cascaded into smaller ones. On the other hand, if the spanwise grid size is small, large eddies are broken into small eddies. The small eddies are more dissipative and thus yield more accurate results of smaller turbulent stresses.

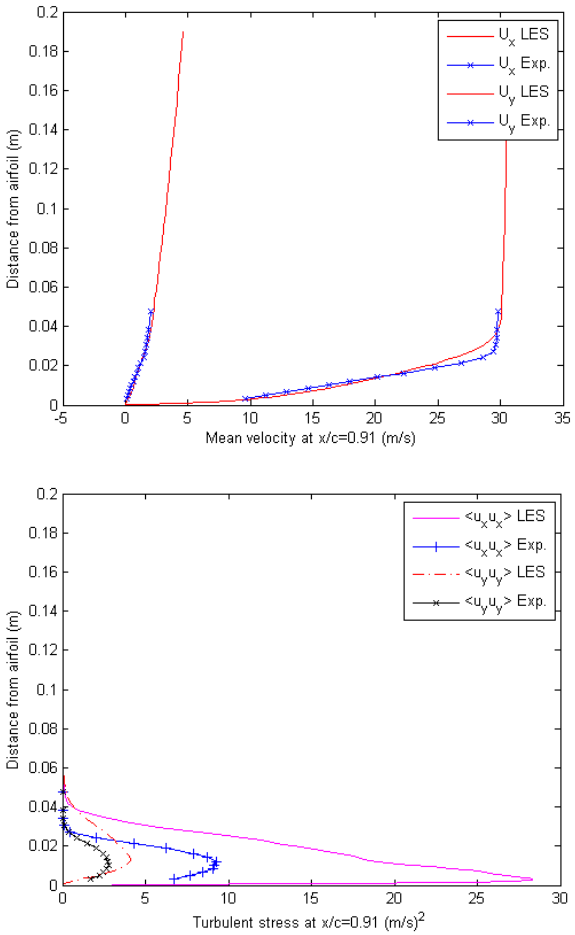

Figure 9. Mean velocity profiles and turbulent stresses.

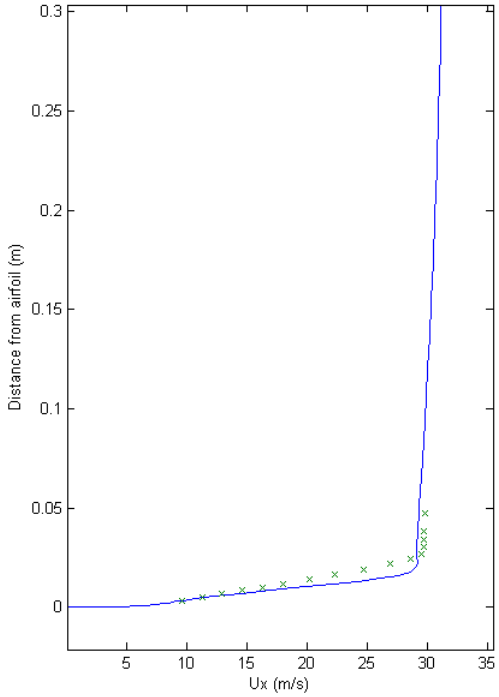

(a)

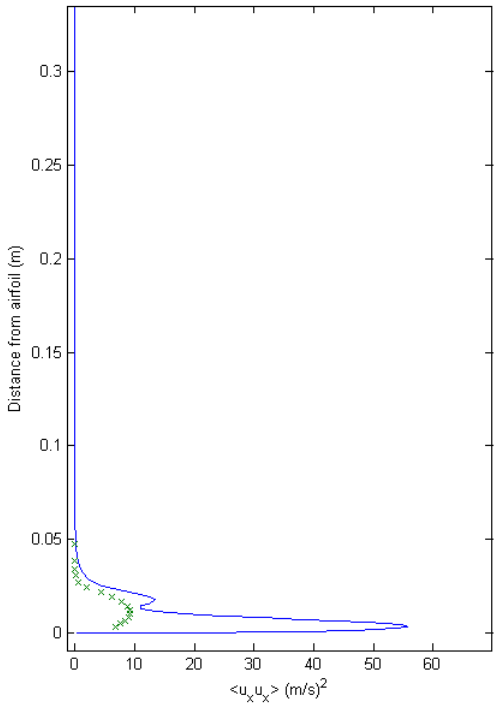

(b)

Figure 10. 2-D results: (a) Streamwise mean velocity profile; (b) Streamwise turbulent stress. -: simulation; x: experiment.

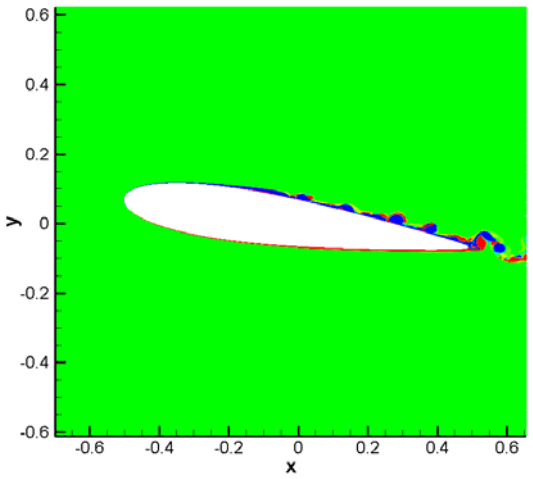

(a)

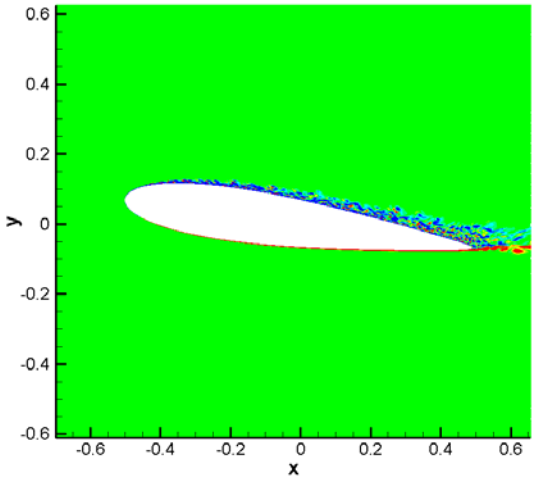

(b)

Figure 11. Instantaneous vorticity plots of (a) 2D computations, and (b) 3D computations.

4 Conclusions

Numerical simulations were carried out for turbulent flow over an NACA 0015 airfoil. The incompressible Navier-Stokes equations are solved using LES with a suitable SGS model. Some simulations were compared with wind tunnel measurements. Results have shown general agreements between simulations and experiments. More investigations were performed with the aim of studying the effect of spanwise grid size. It turns out that too large Δz leads to two-dimensional results, where the spanwise velocity disturbances are poorly modelled.

Acknowledgements

This work was supported by the Energy-Technological Development and Demonstration Programs(EUDP J. nr. 64011-0094 and J. nr. 64009-0272) under the Danish Energy Agency (Energystyrelsen).

References

[1] Baldwin, B.S. and Barth, T.J., "A One Equation Turbulence Transport Model for High Reynolds Number Wall-Bounded Flows", NASA TM 102847,1990.

[2] Spalart, P. R. and Allmaras, S. R., "A One-Equation Turbulence Model for Aerodynamic Flows", *AIAA Paper* 92-0439, 1992.

[3] Launder, B. E., and Sharma, B. I., "Application of the Energy Dissipation Model of Turbulence to the Calculation of Flow Near a Spinning Disc", *Letters in Heat and Mass Transfer*, vol. 1, no. 2, pp. 131-138, 1974.

[4] Wilcox, D.C., "Reassessment of the scale-determing equation for advanced turbulence models", *AIAA Journal*, Vol. 26, No. 11, 1988, 1299-1310.

[5] Spalart, P. R., Jou, W.-H., Stretlets, M., and Allmaras, S. R., "Comments on the Feasibility of LES for Wings and on the Hybrid RANS/LES Approach", Advances in DNS/LES, Proceedings of the First AFOSR International Conference on DNS/LES, 1997.

[6] Smagorinsky, J., "General circulation experiments with the primitive equations", *Mon. Weather Rev*., 91, 99-164, 1963.

[7] Lilly, D.K., "The representation of small-scale turbulence in numerical simulation experiments", Proceedings of the IBM scientific Computing Symposium on Environmental Sciences IBM Form no. 320-1951, 195-210, 1967.

[8] Deardorff, J.W., "A numerical study of three-dimensional turbulent channel flow at large Reynolds numbers", *J. Fluid Mech*., 41, 453-480, 1970.

[9] Bardina J., Ferziger J. H., and Reynolds W., "Improved subgrid scale models for Large-Eddy Simulations", *AIAA paper* No. 80-1357, 1980.

[10] Ta Phuoc L. "Modèles de sous maille appliqués aux ecoulements instationnaires décollés", Proceedings of the DRET Conference, Aérodynamique Instationnaire Turbulente-Aspects Numériques et Expérimentaux, Paris, France, 1994.

[11] P. Sagaut, *Large Eddy Simulation for Incompressible Flows*, *An Introduction*. Springer-Verlag, 1998.

[12] Mary I. and Sagaut P., "Large eddy simulation of flow around an airfoil near stall", *AIAA J.* Vol. 40, No. 6, June 2002.

[13] Piomelli, U., and Balaras, E., "Wall-layer models for large-eddy simulations", *annual review of fluid mechanics*, vol. 34. 2002. pp. 349-374.

[14] Michelsen, J. A., "Basis3D – A Platform for Development of Multiblock PDE Solvers", *Technical Report AFM 1992-05*; Technical University of Denmark.

[15] Michelsen, J. A., "General Curvilinear Transformation of the Navier-Stokes Equations in a 3D Polar Rotating Frame", *Technical Report AFM 1998-01*; Technical University of Denmark.

[16] Sørensen, N. N., "General Purpose Flow Solver Applied Over Hills", *RISØ-R-827-(EN) 1995*; Risø National Laboratory, Denmark.

[17] Shen, W. Z., Michelsen, J. A., and Sørensen, J. N., "An Improved Rhie-Chow Interpolation for Unsteady Flow Computations", *AIAA J*. Vol. 39, No. 12, 2001, pp. 2406-2409. doi:10.2514/2.1252.

[18] Shen, W. Z., Michelsen, J. A., Sørensen, N. N., and Sørensen, J. N., "An Improved SIMPLEC Method on Collocated Grids for Steady and Unsteady Flow Computations", *Numerical Heat Transfer*, Part. B, Vol. 43, No. 3, 2003, pp. 221-239. doi:10.1080/713836202.

[19] Bertagnolio F., "Boundary layer measurements of the NACA 0015 airfoil and Implications for Noise modling", *RISØ-R-1761-(EN) 2011*; Risø National Laboratory, Denmark.